

Nanostructural Characteristics of Vacuum Cold-Sprayed Hydroxyapatite/Graphene-Nanosheet Coatings for Biomedical Applications

Yi Liu, Jing Huang & Hua Li

Journal of Thermal Spray Technology

ISSN 1059-9630

Volume 23

Number 7

J Therm Spray Tech (2014)

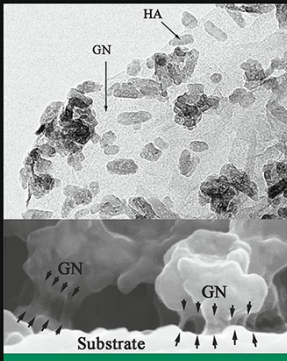
23:1149-1156

DOI 10.1007/s11666-014-0069-2

Volume 23 Number 7 • October 2014

TSS
ASM Thermal Spray Society
An Affiliate Society of ASM International

JOURNAL OF Thermal Spray TECHNOLOGY®



HA
GN
Substrate

INSIDE:

- Photocatalytic Activity of Nanostructured Anatase Coatings
- Cold-Sprayed Nanocomposite Coatings for Biomedical Applications
- Nanocomposite Thermal Barrier Coatings
- Hybrid Processes for Nanocomposite Coating Deposition
- Post-Processing of Nanostructured Coatings
- and much more....

Armelle Vardelle
Lead Editor

Rehan Ahmed
Christopher C. Berndt
Guest Editors

Special Issue: Development and Applications of Nanocomposite Coatings



 Springer

11666 • ISSN 1059-9630
23(7) 1029-1232 (2014)



Your article is protected by copyright and all rights are held exclusively by ASM International. This e-offprint is for personal use only and shall not be self-archived in electronic repositories. If you wish to self-archive your article, please use the accepted manuscript version for posting on your own website. You may further deposit the accepted manuscript version in any repository, provided it is only made publicly available 12 months after official publication or later and provided acknowledgement is given to the original source of publication and a link is inserted to the published article on Springer's website. The link must be accompanied by the following text: "The final publication is available at link.springer.com".



Nanostructural Characteristics of Vacuum Cold-Sprayed Hydroxyapatite/Graphene-Nanosheet Coatings for Biomedical Applications

Yi Liu, Jing Huang, and Hua Li

(Submitted October 14, 2013; in revised form January 22, 2014)

Development of novel biocompatible nanomaterials has provided insights into their potential biomedical applications. Bulk fabrication of the nanomaterials in the form of coatings remains challenging. Here, we report hydroxyapatite (HA)/graphene-nanosheet (GN) composite coatings deposited by vacuum cold spray (VCS). Significant shape changes of HA nanograins during the coating deposition were revealed. The nanostructural features of HA together with curvature alternation of GN gave rise to dense structures. Based on the microstructural characterization, a structure model was proposed to elucidate the nanostructural characteristics of the HA-GN nanocomposites. Results also showed that addition of GN significantly enhanced fracture toughness and elastic modulus of the HA-based coatings, which is presumably accounted for by crack bridging offered by GN in the composites. The VCS HA-GN coatings show potential for biomedical applications for the repair or replacement of hard tissues.

Keywords graphene-nanosheet, hydroxyapatite, microstructure, nanocomposite coatings, vacuum cold spray

1. Introduction

Demand for biomedical implants to correct skeletal defects or substitute for load-bearing hip, knee, and dental endoprosthetics is constantly increasing. It is a prerequisite that the biomaterial for clinical surgery should be capable of withstanding applied physiological forces without substantial dimensional changes, catastrophic brittle fracture, or fracture in the long term from creep, fatigue, or stress corrosion. Development of novel biomaterials and appropriate fabrication techniques is therefore an important research area for improved lifetime, reliability, and bioactive functions of the materials. Thermal-sprayed hydroxyapatite (HA) coatings are nowadays routinely applied on metallic implants to promote fast fixation with bony tissues after surgery (Ref 1-3). However, despite the success of the conventional HA coatings, there are still concerns pertaining to their long-term stability in the human body. Malfunctioning or mechanical failure of the HA-coated implants is a major

concern for coated implants (Ref 4). It is well established that the structural features, e.g., phase composition, crystallinity, Ca/P ratio, grain size, porosity, surface roughness, etc., are related to biocompatibility and mechanical strength of the coatings (Ref 5), which in turn influence their functional service.

Research on bionanotechnology has shed light on the potential application of nanostructured biomaterials (Ref 6-8). Apart from their enhanced mechanical properties, the structural characteristics of the nanomaterials are essential because most tissues have nanoscale features assembled from nanoscale units of amino acids, proteins, and lipids, all of which are in the low end of the nanoscale size range. Yet, a major challenge remains concerning the design and fabrication of appropriate nanostructures. Furthermore, despite excellent biological properties, the inherent brittleness of HA restricts its application in many load-bearing situations (Ref 9-11). Therefore, incorporating second phase reinforcements such as ethylene-based polymers, Ti-alloys, alumina, zirconia, carbon nanotube, and other materials into HA coatings as toughening components has been developed (Ref 12-16). However, few materials that have been considered for HA-based composites satisfy both favorable biocompatibility and sufficient strength. An alternative material, graphene, has been attracting attention due to its unique structural features and appropriate mechanical properties (Ref 17-20). Reports on the biological performance of graphene (Ref 21-23) further imply the possibility of its being an additive in HA for load-bearing biomedical applications, even though the reason for the competitive biocompatibility of graphene remains obscure.

Yi Liu, Jing Huang, and Hua Li, Key Laboratory of Marine Materials and Related Technologies, Zhejiang Key Laboratory of Marine Materials and Protective Technologies, Ningbo Institute of Materials Technology and Engineering, Chinese Academy of Sciences, Ningbo 315201, China. Contact e-mail: lihua@nimte.ac.cn.

Thermal spray is a promising approach for depositing nanostructured biomedical coatings usually by retaining the nanostructures from original feedstock. However, feeding of fine particles, e.g., nano-sized particles, using regular powder feeders usually causes clogging of the hose and results in difficulties in producing sufficient cohesion/adhesion due to the tiny mass of individual particles. Alternative approaches such as agglomeration of micrometer-sized particles (Ref 24) bear challenges in process complexity and microstructural control of the coatings. In addition, thermal spray process is usually accompanied by melting of particles, without which it is hard to fabricate bulk coatings. This raises the concern of how to effectively retain the nanostructural features of the starting powder after the coating formation. Vacuum cold spray (VCS) is an approach based on shock-loading solidification, thereby enabling deposition on various substrates. During VCS processing, ultrafine ceramic particles pass through a micro-orifice nozzle and are accelerated to a high velocity by a carrier gas and subsequently impact on the substrate to form a coating in a vacuum chamber. The room-temperature VCS deposition offers the advantages of efficiently transferring the microstructure of feedstock powder to the as-deposited coating without significant crystal grain growth or structural changes (Ref 25-28).

In this paper, we report nano-HA/graphene-nanosheet (GN) composite coatings deposited by VCS, providing insights into their potential biomedical applications for repair or replacement of hard tissues. Microstructural characterization of the coatings was conducted to elucidate the evolution of the nanostructures. The mechanical properties of the HA-GN coatings were also assessed.

2. Materials and Methods

Large-scale GN was chemically fabricated from high purity flakey graphite via the modified Hummer's method

with further thermal reduction processing. HA powder in nanosizes was synthesized by the wet chemical approach and preparation of the HA-GN powder has been described previously (Ref 29). The morphology of the starting HA-GN composite powder is shown in Fig. 1. HA grains are ~20-45 nm in length and ~10 nm in diameter. The coatings were deposited by VCS onto titanium substrates operated at room temperature. It was realized that during the synthesis, HA nucleated and grew on GN with a preferred orientation. The (300) plane of HA crystal formed a coherent interfacial bond with graphene wall and the section of graphene sheet built a strong interface with (002) plane of HA crystals (Ref 29). These structural features already gave rise to enhanced densification and precluded grain growth of HA in spark plasma-sintered pellets (Ref 29).

Prior to the spraying, the grit-blasted titanium substrates of dimensions of $10 \times 10 \times 1$ mm were rinsed in distilled water and subsequently ultrasonically cleaned in acetone for 30 min. The spray process was carried out using a VCS-2000 system (developed by Xi'an Jiaotong University, China) (Ref 27, 28). A rotary vane vacuum pump coupled to a mechanical booster was used to pump the chamber pressure down to 100-5000 Pa during spraying. Helium gas at a flow rate of 5 l/min was used for feeding and accelerating the powder particles. The scanning speed of 10 mm/s and the spray distance of 10 mm were adopted for the coating deposition.

Microstructure of the powder and the coatings was characterized by transmission electron microscopy (TEM, FEI Tecnai F20, The Netherlands) and field emission scanning electron microscopy (FESEM, S4800, Hitachi, Japan). Phases were characterized by x-ray diffraction (XRD, D8 Advance, Bruker AXS, Germany) using Cu K α radiation ($\lambda = 1.5406 \text{ \AA}$) operated at 40 kV and 40 mA. The goniometer was set at a scan rate of 0.033 $^{\circ}$ /s over a 2θ range of 20° - 60° . The adhesive strength of the coatings was

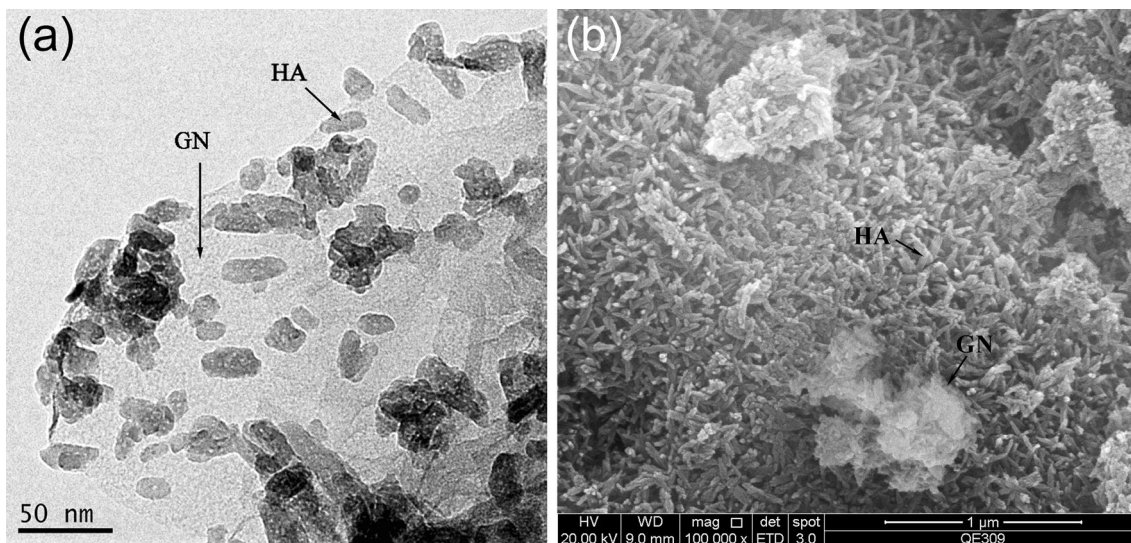
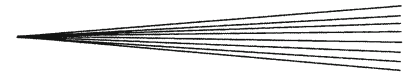


Fig. 1 Morphology of the HA-GN powder showing rod-like HA nanograins attaching on graphene flakes (a) TEM view of the HA-GN powder and (b) FESEM view of the powder



assessed through scratch testing conducted using a micro-scratch tester (MST, WS-2005, China). The acoustic signal of the scratching action was acquired for estimating the adhesion (Ref 30). For the micro-scratch testing, a Rockwell C diamond cone was used to scratch the surface of the coated specimen at a constant speed and under a continuously increasing load. The smallest load at which the coating was damaged, the critical load, L_c , was determined by acoustic emission detection, i.e., by the sudden increase of acoustic emission at certain driving force. Specific surface area and porosity of the VCS coating were measured by the N_2 adsorption-desorption method (Micromeritics ASAP 2020, USA). The porosity was calculated as the fraction of the total pore volume to the total coating volume. Surface roughness was measured with a surface profiler, a scanning mechanical microscope (Alpha-Step IQ, KLA-Tencor, USA) with a vertical resolution of 0.012 \AA . The measurement was made based on an inductive sensor equipped with a diamond stylus probe with a pyramidal shape of $5 \mu\text{m}$ in radius and a vertex angle of 60° . A scan speed of $50 \mu\text{m/s}$ over a scan length of $1000 \mu\text{m}$ was used.

Fracture toughness (K_{IC}) of the coatings was determined by using the indentation approach. The test was conducted on Micro-Vickers microhardness tester (HV-1000, Shanghai Lianer Testing Equipment Corporation,

China). A 300 gf Vickers load was applied on the polished cross-sections of the coatings with a loading time of 10 s. A total of ten points were collected for each sample. K_{IC} was calculated through the Anstis equation (Ref 31): $K_{IC} = 0.016(E/H)^{1/2}(P/C^{3/2})$, where P is load, C is crack length, H is microhardness, and E is elastic modulus. The Vickers microhardness of the coatings was measured from their polished cross-sections using the Micro-Vickers microhardness tester with a load of 300 g and the loading duration of 15 s. The elastic modulus was determined by means of nano-indentation test conducted using a nano-mechanical test system (NANO G200, MTS, USA) with a standard Berkovich indenter. The maximum indentation depth chosen for the present test was $1 \mu\text{m}$. Six indentations were made for each test.

3. Results and Discussion

Nanostructured HA and HA-GN coatings with tunable thickness were deposited by VCS. The surface of the coatings exhibits similar nanostructural features for the coatings with and without addition of GN (Fig. 2a-c), that is, the coatings demonstrate micrometer-sized pits and protrusions on their surfaces. This presumably indicates rebounding of certain HA nanoparticles upon their

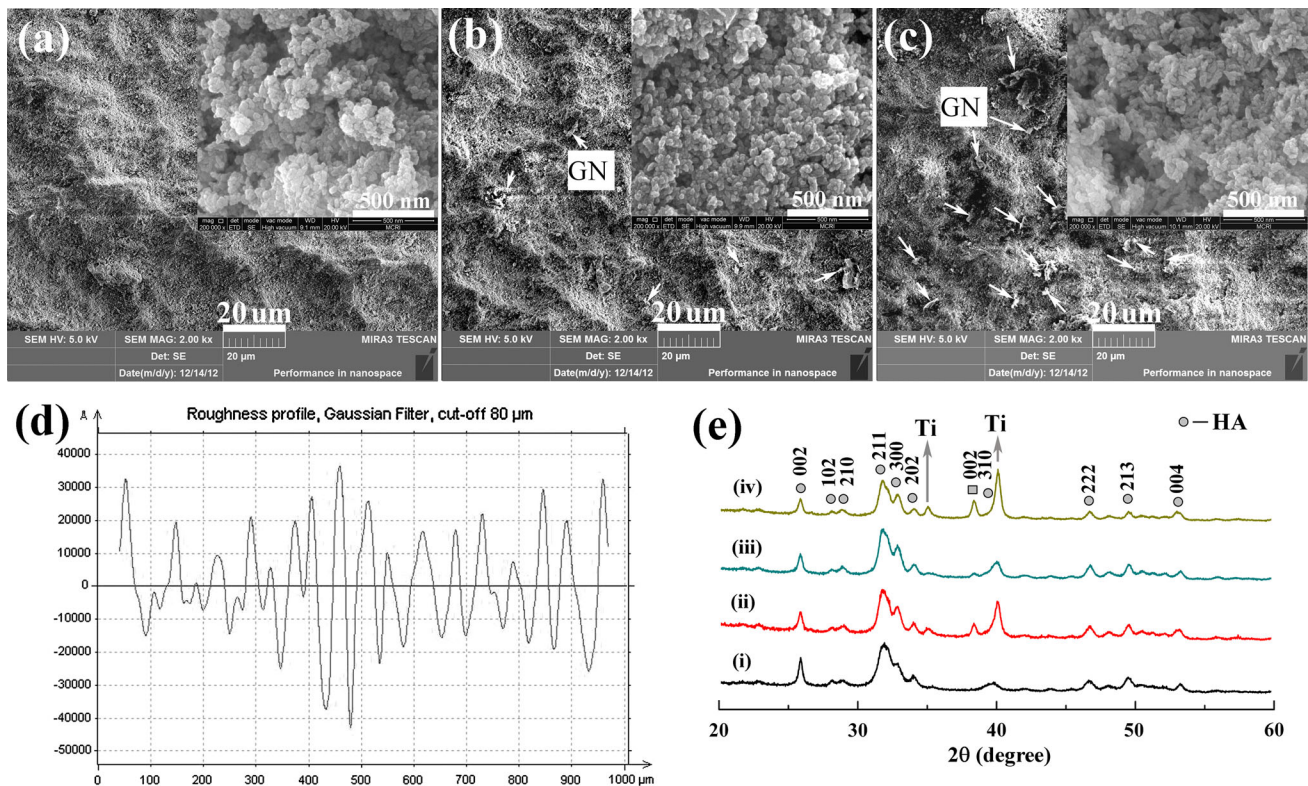


Fig. 2 Topographical morphology, surface profile, and XRD spectra of the HA-based coatings (a-c) FESEM top views of the as-deposited nanostructured coatings, enlarged view of selected area is also shown on the top-right corner of each picture (a: the pure HA coating, b: the HA-0.1 wt.%GN coating, and c: the HA-

1.0 wt.%GN coating), (d) surface roughness profile of the typical HA-1.0 wt.%GN coating, and (e) XRD peaks of the powder and coatings (the peaks for Ti were detected from the substrate, i: the starting HA powder, ii: the pure HA coating, iii: the HA-0.1 wt.%GN coating, and iv: the HA-1.0 wt.%GN coating)

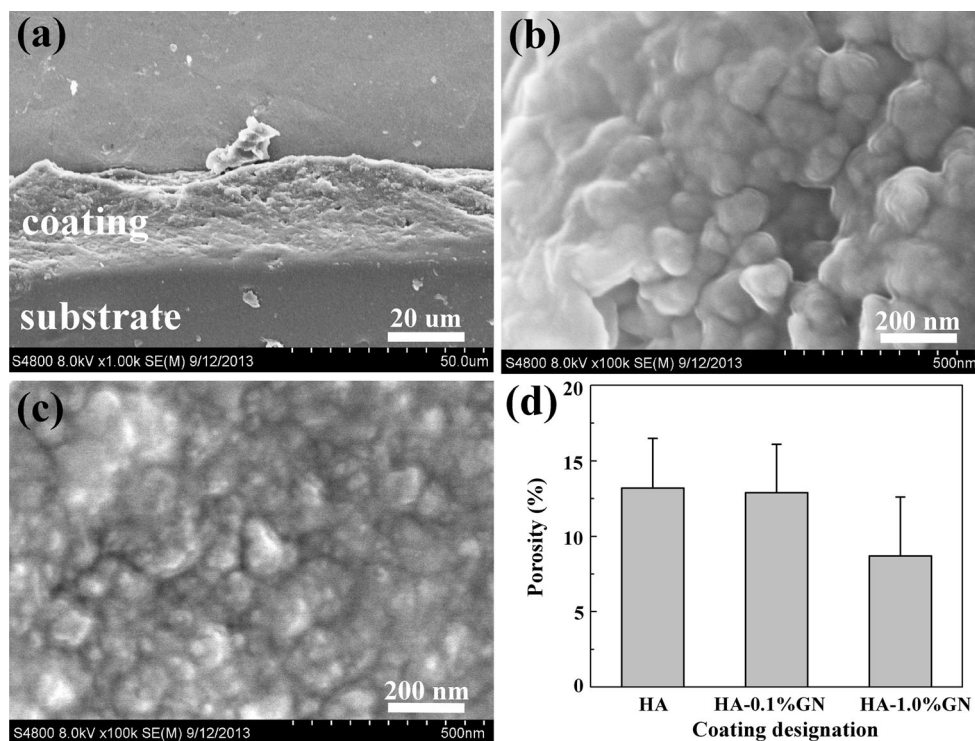


Fig. 3 Cross-sectional morphology (a) and porosity (d) of the coatings (b and c are enlarged views of the selected areas in a). The porosity of five coating samples was measured for each type of the coatings for an average value

impingement during the coating formation stage, which is usual for the cold spray deposition (Ref 32). Surface roughness profile discloses the rough surface of the nanocomposite coatings in micrometer sizes (Fig. 2d), i.e., a R_a of 1.09 μm . It has been established that some degree of surface roughness of biomaterials is critical in affecting the adhesion and growth of cells (Ref 33, 34). Usually high surface roughness enhances body-fluid interaction by altering the surface wettability and free energy, which favors adsorption of serum proteins (Ref 34).

As noticed from the topographical views of the coatings (shown at top-right corners of Fig. 2a-c), randomly oriented small HA crystallites in the size of <20 nm can be distinguished, which are comparable to the starting rod-like HA grains. Homogeneously dispersed graphene flakes are also seen on the coating surfaces. XRD detection verifies the well-retained structure of the starting HA-GN after the VCS processing (Fig. 2e). XRD detection did not show the trace of graphene in the samples, which is very likely due to the special structural feature of graphene. Compared with the starting feedstock, the coatings show no changes in the phases. This is not surprising since the coating deposition was operated at room-temperature. Peak broadening is attributed to the retention of the nano-sized crystals in the powder. No new peaks for the as-sprayed coatings are shown. It is acknowledged that microstructure, crystallinity, and phase composition of HA coatings are critical in deciding behaviors of the cells attached/proliferated on them (Ref 5). The entirely retained crystalline HA in the HA-GN nanocomposite

coatings would favor their biocompatibility, which can be translated into enhanced adhesion and reproduction of the cells on their surfaces.

Cross-sectional views of the coatings display randomly oriented polycrystalline HA grains smaller than 50 nm and the grains are tightly connect with each other (Fig. 3a-c). Compared to the starting feedstock particles (Fig. 1), changes in grain size and morphology of HA grains are seen. No more rod-like grains are observed, instead, HA grains of spherical shape exist in the coating. Previous XRD profiles (Fig. 2e) already showed increased intensity ratio of (300) peak to (002) peak for the VCS coatings compared to that of the starting powder, thereby implying preferred crystallographic orientation of HA. This change is likely due to a reduction in crystal size and/or distortion of HA particles during the deposition, which agrees well with the morphological changes of HA (Fig. 3b, c versus 1).

The size of certain HA grains in the coatings, <20 nm, is smaller than that of the starting particles. This is likely attributed to collision-induced breakage (Ref 26). During the room-temperature VCS deposition, local temperature increase could not result in ceramic sintering and particle melting during impingement. The reduction in crystallite size resulting from fracture or plastic deformation during the VCS process is predominately responsible for the dense structure of the coatings. In fact, similar plastic deformation of alumina particles during VCS processing has been reported (Ref 25). It was reported that the maximum local temperature rise and the shock pressure at the point of impact between particle and substrate during

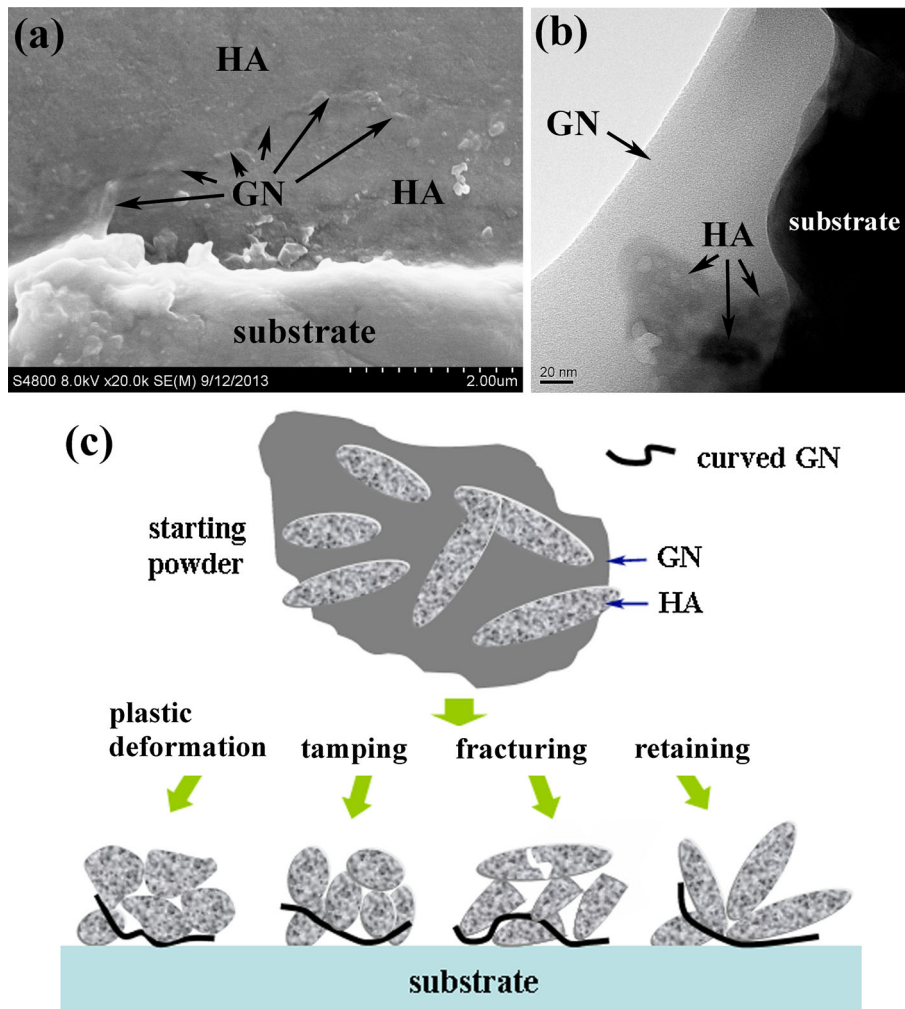


Fig. 4 FESEM (a) and TEM (b) images of the HA-GN coating showing presence of GN in the first layer that intimately contacts with the substrate, and (c) schematic illustration demonstrating the formation mechanisms of the HA-GN nanocomposite coating

alumina layer formation did not exceed 500 °C and 2.5 GPa (Ref 26). The local compact pressure is almost enough to induce plastic deformation and fracture of ceramic particles. The impact of feedstock particles with high velocity onto the substrate likely introduces high local compact pressure and high strain rate of colliding particles which mainly affects the dislocation motion related to plastic deformation of the vacuum cold-sprayed particles. This densification regime for ceramic particles during VCS processing is different from conventional shock compaction, which might give rise to favorable properties.

Porosity is a key variable that determines the specific area in contact with the physiological medium and, therefore, influences physiochemical interactions at the implant-host interface. Porosity measurements showed the average porosity of 13.2, 12.9, and 8.7% for the HA coating, the HA-0.1 wt.%GN coating, and the HA-1.0 wt.%GN coating, respectively (Fig. 3d). In addition, the BET result suggests a pore size range of 2-8 nm. Apparently, the addition of GN results in a denser

structure. During VCS processing, it is possible that the particles with high impingement speed yield acceptable consolidation at room temperature without the need for thermal treatment. This process has been termed room-temperature impact consolidation (Ref 26). Consolidation features of the current HA-GN composites are fundamentally similar to those fabricated by the shock compaction method (Ref 35, 36).

Further microstructural examination from the cross-sections of the coatings suggests that apart from its even distribution within the coatings, GN stays in the first layer intimately contacting with the substrate (Fig. 4a, b). GN stretches from the coating/substrate interface all the way to the inner coating (Fig. 4a), which should benefit adhesion/cohesion of the coating. The particular structural feature of the starting HA-GN composites (Fig. 1) is apparently retained in the coating that individual HA grains still affiliate to GN (Fig. 4b). Based on the microstructural observations, a schematic depiction is proposed illustrating the formation regimes of the HA-GN coatings (Fig. 4c). The shape changes of the rod-like HA grains

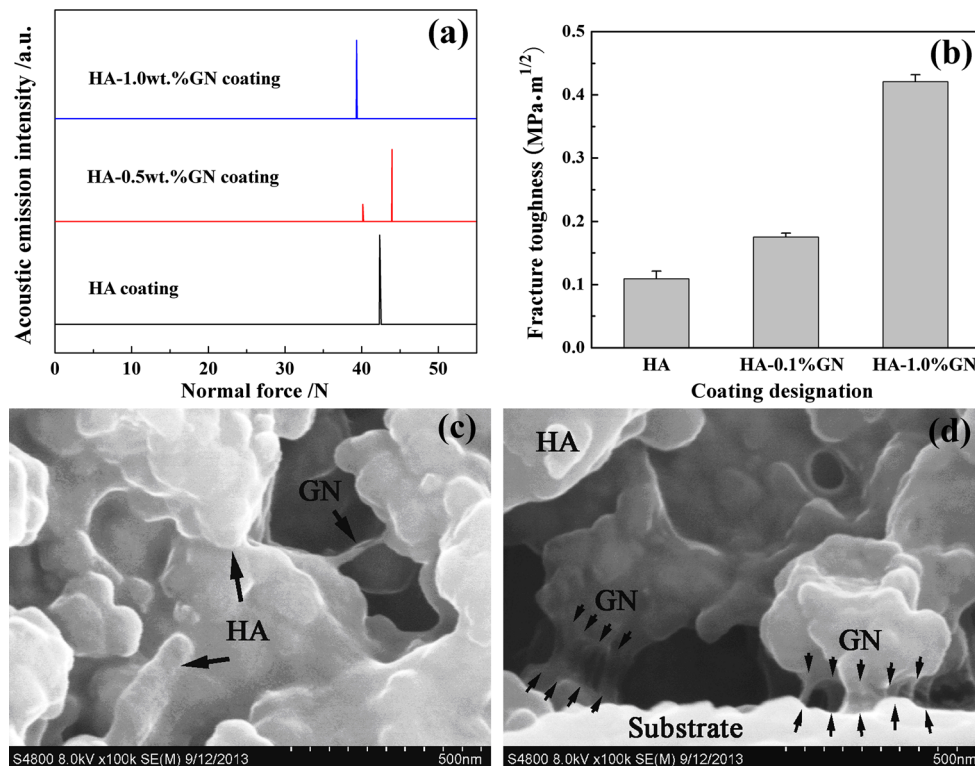


Fig. 5 Adhesion testing curves acquired by measuring the normal force for the HA and the HA-GN composite coatings (a), and fracture toughness of the coatings (b). Microstructural character-

ization by FESEM revealed the toughening regime of crack bridging accomplished by GN in the HA-GN composite coating (c, d)

seem to be retaining, fracturing, plastic deformation, and tamping. The starting nano-sized particles tend to agglomerate due to their high specific surface energy. During the VCS process, the loosely agglomerated particles successively impact on the substrate to form the first layer and their high kinetic energy results in further consolidation. GN attains intimate contact with the substrate and its curvature changes were realized. Due to the brittle nature of HA, fracture of HA grains likely happens at this stage. Following tamping by the collision of subsequent particles further makes the former layer compact and denser. The tamping effect alone could also trigger shape changes of HA grains. Plastic deformation of ceramic particles at room temperature might be normal at the initial stage, because VCS is capable of making coatings for a large variety of ceramics. It is anticipated that during later stages of coating deposition, fracturing plays more important role accounting for the shape changes of HA grains, since as a ceramic material, HA possesses poor capability of plastic deformation. This speculation still needs further experimental verification.

Sufficient mechanical properties are essentially required for long-term functional services of HA-coated implants. The adhesion of biomedical coating to substrate is one of the crucial factors that affect its functions after surgery (Ref 37). The presence of GN at coating/substrate interface and within the coatings might influence their cohesion/adhesion. However, according to the acoustic emission versus critical load curves for the coatings

(Fig. 5a), the average normal force ranges from 20 to 45 N, showing irrelevance to content of GN in the coatings. The adhesion values of the HA-GN composite coatings are competitive as compared to those exhibited by other HA-based coatings, e.g., pulsed laser-deposited HA coating on Ti-based implants showed the value of 10.77 N (Ref 38). This nevertheless suggests that GN existing at coating/substrate interface is not detrimental to the bonding of the coating to the substrate. The cross-sectional morphologies of the coatings already show dense microstructure and GN stays in the first layer that intimately contacts with the substrate (Fig. 4). During the scratch testing, GN or HA particles might be peeled off by the diamond probe, in turn resulting in the acoustic emission. The critical load that triggered acoustic emission may be influenced by varied features of the coatings, such as surface roughness, thickness, composition homogeneity, etc. The theory behind the irrelevance between critical load and content of GN in the coatings is unknown yet, which needs further clarification.

On the other hand, the microhardness and elastic modulus of the coatings are improved by the addition of GN (Fig. 5b). The fracture toughness (K_{IC}) of the HA-1.0 wt.%GN composite reaches 0.42 MPa m^{1/2}, showing ~280% improvement compared to that of the pure HA coating, 0.11 MPa m^{1/2}. The microhardness and elastic modulus of the HA-1.0 wt.%GN coating are 0.22 and 4.25 GPa, respectively, showing marked increase compared to those of the pure HA coating, 0.17 and 3.05 GPa. An



appropriate elastic modulus for coated implant is crucial in order to avoid stress shielding and bone resorption, and it also determines fatigue behavior of the coatings under cyclic loading. The elastic modulus of the HA-GN coating is closer to that of human skeletal bone (~10 GPa).

The toughening mechanisms of the HA-GN nanocomposites are important issues that are worth extensive research efforts. The predominate toughening mechanisms in spark plasma-sintered HA-GN nanocomposites are pullout of GN, crack deflection at the HA-GN interface, and crack bridging by GN (Ref 29). For the cold-sprayed HA-GN composites, the toughening mechanism might be different from the sintered ones. Crack bridging offered by GN is clearly seen (Fig. 5c, d). Individual GN bridges the gap between HA particles and the coating/substrate interface as well (Fig. 5d), preventing effectively widening of the crack. It is noted that GN remains intact in the coating, providing toughening via restraining the crack tip from opening and propagating further. Even though the significantly enhanced mechanical properties already give insight into potential biomedical applications of the HA-GN nanocomposite coatings, it should be noted that prior to being considered for biomedical applications, the biological properties of the coatings must be systematically evaluated. Previous research findings on in vitro behaviors of graphene (Ref 21-23) and HA-GN composites (Ref 29) have shown satisfactory bio-performances of the composites. Part of our ongoing research efforts are being devoted to adsorption behavior of key serum proteins on the HA-GN coatings and subsequent cell behaviors.

4. Conclusions

HA/GN nanocomposite coatings with micrometer-sized surface roughness and tunable thickness were fabricated by VCS. Competitive adhesion/cohesion of the coatings was achieved. Changes of curvature of GN and contours of HA nanograins were disclosed after the spraying. The phases in the starting HA-GN composites were completely retained in the coatings. Starting rod-like HA grains presumably experienced retaining, fracturing, tamping, and plastic deformation. GNs are evenly dispersed in the coatings and at the coating/substrate interface, resulting in remarkably enhanced fracture toughness. Crack bridging accomplished by GN was disclosed as the predominant toughening regime. The results shed some light on potential applications of GN as additives for biomedical nanocomposites.

Acknowledgments

This research was supported by the National Natural Science Foundation of China (Grant # 31271017) and 100 Talents Program of Chinese Academy of Sciences (both to H.L.). The authors thank Drs. Yuyue Wang and Zhaohui

Dang from Xi'an Jiaotong University, China for their technical help in making the coatings by VCS.

References

1. R.G.T. Geesink, K. de Groot, and C.P. Klein, Bonding of Bone to Apatite-Coated Implants, *J. Bone Joint Surg.*, 1988, **70B**, p 17-22
2. S.D. Cook, K.A. Thomas, J.F. Dalton, T.K. Volkman, T.S. Whitecloud, III, and J.F. Kay, Hydroxyapatite Coating of Porous Implants Improves Bone Ingrowth and Interface Face Attachment Strength, *J. Biomed. Mater. Res.*, 1992, **26**, p 989-1001
3. P.K. Stephenson, M.A. Freeman, P.A. Revell, J. Germain, M. Tuke, and C.J. Pirie, The Effect of Hydroxyapatite Coating on Ingrowth of Bone into Cavities in An Implant, *J. Arthroplasty*, 1991, **6**, p 51-58
4. J.E. Dalton and S.D. Cook, In Vivo Mechanical and Histological Characteristics of HA-Coated Implants Vary with Coating Vendor, *J. Biomed. Mater. Res.*, 1995, **29**, p 239-245
5. L. Sun, C.C. Berndt, K.A. Gross, and A. Kucuk, Material Fundamentals and Clinical Performance of Plasma Sprayed Hydroxyapatite Coatings: A Review, *J. Biomed. Mater. Res.*, 2001, **58**, p 570-592
6. T.J. Webster, R.W. Siegel, and R. Bizios, Osteoblast Adhesion on Nanophase Ceramics, *Biomaterials*, 1999, **20**, p 1221-1227
7. L.G. Gutwein and T.J. Webster, Increased Viable Osteoblast Density in the Presence of Nanophase Compared to Conventional Alumina and Titania Particles, *Biomaterials*, 2004, **25**, p 4175-4183
8. T.J. Webster, C. Ergun, R.H. Doremus, R.W. Siegel, and R. Bizios, Enhanced Functions of Osteoblasts on Nanophase Ceramics, *Biomaterials*, 2000, **21**, p 1803-1810
9. Y.W. Gu, N.H. Loha, K.A. Khor, S.B. Tor, and P. Cheang, Spark Plasma Sintering of Hydroxyapatite Powders, *Biomaterials*, 2002, **23**, p 37-43
10. H. Li, K.A. Khor, and P. Cheang, Titanium Dioxide Reinforced Hydroxyapatite Coatings Deposited by High Velocity Oxy-Fuel (HVOF) Spray, *Biomaterials*, 2002, **23**, p 85-91
11. S. Saber-Samandari and K.A. Gross, Amorphous Calcium Phosphate Offers Improved Crack Resistance: A Design Feature from Nature?, *Acta Biomater.*, 2011, **7**, p 4235-4241
12. S. Velayudhan, T.V. Anilkumar, T.V. Kumary, P.V. Mohanan, A.C. Fernandez, H.K. Varma, and P. Ramesh, Biological Evaluation of Pliable Hydroxyapatite-Ethylene Vinyl Acetate Co-polymer Composites Intended for Cranioplasty, *Acta Biomater.*, 2005, **1**, p 201-209
13. H. Li, K.A. Khor, and P. Cheang, Impact Formation and Structure Characterization of Thermal Sprayed Hydroxyapatite/Titania Composite Coatings, *Biomaterials*, 2003, **24**, p 949-957
14. J. Li, B. Fartash, and L. Hermansson, Hydroxyapatite-Alumina Composites and None-Bonding, *Biomaterials*, 1995, **16**, p 417-422
15. H. Li, K.A. Khor, R. Kumar, and P. Cheang, Characterization of Hydroxyapatite/Nano-zirconia Composite Coatings Deposited by High Velocity Oxy-fuel (HVOF) Spray Process, *Surf. Coat. Technol.*, 2004, **182**, p 227-236
16. D. Zhang, C. Yi, J. Zhang, Y. Chen, X. Yao, and M. Yang, The Effects of Carbon Nanotubes on the Proliferation and Differentiation of Primary Osteoblasts, *Nanotechnology*, 2007, **18**, p 475102-475110
17. K.S. Novoselov, D. Jiang, F. Schedin, T.J. Booth, V.V. Khotkevich, S.V. Morozov, and A.K. Geim, Two-Dimensional Atomic Crystals, *Proc. Natl. Acad. Sci. USA*, 2005, **102**, p 10451-10453
18. S. Stankovich, D.A. Dikin, G.H.B. Dommett, K.M. Kohlhaas, E.J. Zimney, E.A. Stach, R.D. Piner, S.T. Nguyen, and R.S. Ruoff, Graphene-Based Composite Materials, *Nature*, 2006, **442**, p 282-286
19. T. Ramaniathan, A.A. Abdala, S. Stankovich, D.A. Dikin, M. Herrera-Alonso, R.D. Piner, D.H. Adamson, H.C. Schniepp, X. Chen, R.S. Ruoff, S.T. Nguyen, I.A. Aksay, R.K. Prud'homme, and L.C. Brinson, Functionalized Graphene Sheets for Polymer Composites, *Nat. Nanotechnol.*, 2008, **3**, p 327-331

20. L.S. Walker, V.R. Marotto, M.A. Rafiee, N. Koratkar, and E.L. Corral, Toughening in Graphene Ceramic Composites, *ACS Nano*, 2011, **5**, p 3182-3190
21. C. Chung, Y.K. Kim, D. Shin, S.R. Ryoo, B.H. Hong, and D.H. Min, Biomedical Applications of Graphene and Graphene Oxide, *Acc. Chem. Res.*, 2013, **46**, p 2211-2224
22. Y. Wang, Z.H. Li, J. Wang, J.H. Li, and Y.H. Lin, Graphene and Graphene Oxide: Biofunctionalization and Applications in Biotechnology, *Trends Biotechnol.*, 2011, **29**, p 205-212
23. H. Shen, L.M. Zhang, M. Liu, and Z.J. Zhang, Biomedical Applications of Graphene, *Theranostics*, 2012, **2**, p 283-294
24. R.S. Lima and B.R. Marple, Superior Performance of High-Velocity Oxyfuel-Sprayed Nanostructured TiO₂ in Comparison to Air Plasma-Sprayed Conventional Al₂O₃-13TiO₂, *J. Therm. Spray Technol.*, 2005, **14**, p 397-404
25. J. Akedo, Aerosol Deposition Method for Fabrication of Nano Crystal Ceramic Layer-Novel Ceramics Coating with Collision of Fine Powder at Room Temperature, *Mater. Sci. Forum*, 2004, **449-452**, p 43-48
26. J. Akedo, Room Temperature Impact Consolidation (RTIC) of Fine Ceramic Powder by Aerosol Deposition Method and Applications to Microdevices, *J. Therm. Spray Technol.*, 2008, **17**, p 181-198
27. Y.Y. Wang, Y. Liu, C.J. Li, G.J. Yang, and K. Kusumoto, Electrical and Mechanical Properties of the Nanostructure TiN Coatings Deposited by Vacuum Cold Spray, *Vacuum*, 2012, **86**, p 953-959
28. Y. Liu, Y.Y. Wang, G.J. Yang, J.J. Feng, and K. Kusumoto, Effect of Nano-sized TiN Additions on the Electrical Properties of Vacuum Cold Sprayed SiC Coatings, *J. Therm. Spray Technol.*, 2010, **19**, p 1238-1243
29. Y. Liu, J. Huang, and H. Li, Synthesis of Hydroxyapatite-Reduced Graphite Oxide Composites for Biomedical Applications: Oriented Nucleation and Epitaxial Growth of Hydroxyapatite, *J. Mater. Chem. B*, 2013, **1**, p 1826-1834
30. A.J. Perry, Scratch Adhesion Testing of Hard Coatings, *Thin Solid Films*, 1983, **107**, p 167-180
31. G.R. Anstis, P. Chantikul, B.R. Lawn, and D.B. Marshall, A Critical Evaluation of Indentation Techniques for Measuring Fracture Toughness: I, Direct Crack Measurements, *J. Am. Ceram. Soc.*, 1981, **64**(9), p 533-538
32. Y.Y. Wang, Y. Liu, C.J. Li, G.J. Yang, J.J. Feng, and K. Kusumoto, Investigation on the Electrical Properties of Vacuum Cold Sprayed SiC-MoSi₂ Coatings at Elevated Temperatures, *J. Therm. Spray Technol.*, 2011, **20**(4), p 892-897
33. H.H. Huang, C.T. Ho, T.H. Lee, T.L. Lee, K.K. Liao, and F.L. Chen, Effect of Surface Roughness of Ground Titanium on Initial Cell Adhesion, *Biomol. Eng.*, 2004, **21**, p 93-97
34. D.D. Deligianni, N.D. Katsala, P.G. Koutsoukos, and Y.F. Missirlis, Effect of Surface Roughness of Hydroxyapatite on Human Bone Marrow Cell Adhesion, Proliferation, Differentiation and Detachment Strength, *Biomaterials*, 2001, **22**, p 87-96
35. F. Gärtner, T. Stoltenhoff, T. Schmidt, and H. Kreye, The Cold Spray Process and Its Potential for Industrial Applications, *J. Therm. Spray Technol.*, 2006, **15**(2), p 892-897
36. S. Romankov, Y. Hayasaka, G. Kalikova, S.V. Komarov, N. Hayashia, and E. Kasai, TEM Study of TiN Coatings Fabricated by Mechanical Milling Using Vibration Technique, *Surf. Coat. Technol.*, 2009, **203**, p 1879-1884
37. Y. Duan, S. Zhu, F. Guo, J. Zhu, M. Li, J. Ma, and Q. Zhu, The Effect of Adhesive Strength of Hydroxyapatite Coating on the Stability of Hydroxyapatite-Coated Prostheses in Vivo at the Early Stage of Implantation, *Arch. Med. Sci.*, 2012, **8**, p 199-208
38. M. Komath, P. Rajesh, C.V. Muraleedharan, H.K. Varma, R. Reshmi, and M.K. Jayaraj, Formation of Hydroxyapatite Coating on Titanium at 200°C Through Pulsed Laser Deposition Followed by Hydrothermal Treatment, *Bull. Mater. Sci.*, 2011, **34**, p 389-399